A phenomenological model for predicting the early development of the flame kernel in spark-ignition engines

A phenomenological model for predicting the early development of the flame kernel in spark-ignition engines

Pietro Giannattasio, Marco Pretto, Enrico De Betta

Dipartimento Politecnico di Ingegneria e Architettura, Università degli Studi di Udine, Via delle Scienze 206, 33100, Udine, Italy

e-mail addresses: pietro.giannattasio@uniud.it; marco.pretto@uniud.it; debetta.enrico@spes.uniud.it

Abstract. This work presents a simple and effective phenomenological model for the prediction of the early growth of the flame kernel in SI engines, including its initiation as a result of the electrical breakdown of the fuel/air mixture between the spark plug electrodes. The present model aims to provide an improved description of the ignition-affected early phases of flame kernel development compared to the majority of models currently available in literature. In particular, these models focus on electrical energy supply and turbulence, whereas the stretch-induced kernel growth slowdown is quantified with linear models that are inconsistent with the small kernel radius. For the flame kernel initiation, this model replaces the current methods that rely on 1D heat diffusion within a plasma column with a more consistent analysis of post-breakdown conditions. Concerning the kernel growth, the present model couples the mass and energy conservation equations of a spherical kernel with the species and temperature profiles outside of it. This combination leads to a non-linear description of the flame stretch, according to which the kernel development is controlled by the Lewis-number-dependent balance between the heat gained via combustion and the heat lost via thermal diffusion. As a result, the kernel temperature differs from the adiabatic flame temperature, causing the laminar flame speed to change from its adiabatic value and ultimately affecting the overall kernel development. Kernel growth predictions are conducted for laminar flames and compared to literature data, showing a satisfactory agreement and highlighting the ability to describe the stretch-induced kernel slowdown, up to its possible extinction. A good agreement with literature data is also obtained for kernel expansions under moderately turbulent conditions, typical of internal combustion engines. The simple formulation of the present model enables swift integration into phenomenological combustion models for spark-ignition engines, while simultaneously offering useful insight into the early kernel development even for CFD-based approaches.

1. Introduction

Understanding and modelling the ignition and early growth of the flame kernel in SI engines has been a topic of interest for many years. Early simulations of spark discharges in air date back to the 1970s [1], followed by seminal contributions from Maly and co-workers on the effect of spark ignition on reactive mixtures [2] [3]. The latter identified the presence of a sub-100 ns breakdown phase followed by an arc and/or glow discharge, as well as the super-adiabaticity of the resulting flame kernel and the consequently increased growth rate. Modelling of these effects was carried out a few years later, when several kernel development models based on mass and energy conservations were proposed. Notable among these is Herweg and Maly's model [4], which describes the kernel mass increase as

$$\frac{dm_k}{dt} = \rho_u A_k \left(S_T + S_{plasma}\right). \tag{1}$$

Turbulent flame speed S_T is computed from $S_{L,adf}$ using the BML turbulence model, whereas S_{plasma} derives from a 1D heat conduction equation and accounts for the super-adiabatic kernel. The core of this method is the superposition of flame speeds, and it lends itself well to an implementation into full SI combustion models, possibly adopting the simplification for which S_{plasma} is only due to the electrical energy supply [5]. A similar model was proposed by Shen et al. [6], who estimated the end-of-breakdown conditions according to Refael and Sher [7] and described the early kernel development as the sequence of a heat diffusion phase (associated with S_{plasma}) and a flame propagation phase (associated with S_T). The former is arbitrarily ended at $T_k < 3T_{adf}$, and the remaining contribution, S_T, is computed assuming $S_L > S_{L,adf}$ due to $T_k > T_{adf}$. This model has been applied with minimal variations [8] [9] and further developed as a Lagrangian kernel initiation sub-model for implementation into CFD-based combustion models for SI engines [10] [11] [12].

Despite their widespread adoption, these models present two key limitations. The first one lies in the breakdown phase, where the very fast energy deposition between the electrodes causes a massive increase in pressure and temperature and the formation of a plasma column. Then, a shockwave is released and the plasma cools down interacting with the environment. The post-shockwave conditions are computed assuming a near-instantaneous expansion to p_u of a constant plasma mass, yielding [7]:

$$\begin{cases} T_{ig} = T_0 \left[\frac{1}{\gamma}\left(\frac{T_{bd}}{T_0} - 1\right) + 1\right], & \text{(2a)} \\ d_{ig} = 2\left[\frac{\gamma - 1}{\gamma} \cdot \frac{E_{bd}}{\pi p_u d_{gap}\left(1 - T_0/T_{ig}\right)}\right]^{\frac{1}{2}}. & \text{(2b)} \end{cases}$$

Assuming $T_{bd} \cong 45{,}000$ K and $\gamma = 5/3$, equation (2a) yields $T_{ig} \cong 27{,}000$ K, which is too high a value for combustion to play a meaningful role. For this reason, a pure heat diffusion model is adopted to relax the kernel temperature down to $T_k = 3T_{adf}$ in a process that takes about 10 µs after the breakdown, before starting the actual flame kernel modelling. However, simulations of plasma expansion [13] show that it takes up to 5 µs to reach near-uniform pressure, and that in the same timeframe combustion heat release is not negligible.

The second limitation is the flame stretch modelling, which is performed assuming that the flame temperature never goes below T_{adf}, and that the flame speed decreases linearly according to stretch factor I_0. For example, in [4] I_0 is

$$I_0 = \frac{S_{L,stretched}}{S_L} = 1 - \left[\left(\frac{\delta_L}{15L}\right)^{\frac{1}{2}}\left(\frac{u'}{S_L}\right)^{\frac{3}{2}} + \frac{2\delta_L}{S_L r_k}\frac{dr_k}{dt}\right] \cdot \left[\frac{1}{Le} + \left(\frac{Le - 1}{Le}\right)\frac{T_a}{2T_{adf}}\right]. \tag{3}$$

Expression (3) and similar ones, albeit convenient, are inconsistent with many observations on the sub-adiabaticity [14] and non-linear behavior of stretched premixed flames [15] [16], which indicate that the minimum radius for proper linear modelling of stretch is $r_k \cong 8$ mm. Additionally, the key mechanism leading to flame extinction is large heat loss towards the unburned mixture [17], ignored by such models. Aware of this, researchers have tackled flame initiation on more solid theoretical foundations [18], proposing thermo-diffusive 1D kernel expansion models that include profiles of temperature and reactants inside and outside the kernel, as well as electrical energy deposition [19]. However, the thermo-diffusive assumption of constant density prevents the attainment of quantitative results, and such models cannot capture the complex effects of turbulence, which require at least dedicated sub-models [20] if not, especially for turbulence-flame interaction, CFD approaches [21]. The stochastic nature of turbulence is also a key reason behind cycle-to-cycle variation [22], and CFD has proved helpful also in this regard [23], albeit at the cost of heavy computational burden.

Finally, although flame initiation plays a key role in ICEs, successful phenomenological modelling of SI engines is possible even in the absence of dedicated ignition sub-models [24] [25] [26]. However, this lack leads to mispredictions around the ignition phase [27], and it is in this framework that the present paper intends to contribute by proposing a phenomenological model of the early flame kernel development in SI engines. This model combines mass and energy conservations with thermo-diffusive relations to provide accurate kernel growth predictions. Inspiration comes from the work of Ko et al. [28] [29], but independent development conducted by the authors has led to a much simpler and easily replicable model. The target is to include this model and its future developments into phenomenological SI combustion models, although some of its elements may find application even in the flame initiation in CFD environments.

The paper is structured as follows. Section 2 presents the kernel growth model, focusing first on the initial conditions and then on the kernel expansion. The results are reported and compared with available data in Section 3 for a variety of laminar and turbulent cases. Conclusions and future developments are presented in Section 4.

2. Methodology

2.1. Initial conditions: the breakdown model

As stated in Section 1, the typical modelling of post-breakdown conditions appears inconsistent with dedicated plasma simulations, and two major points of concern should be raised. Firstly, the widely used equations (2a) and (2b) are inadequate: this was already shown by Sher and co-workers [30], who obtained for air in atmospheric conditions a final plasma column diameter of $d_{ig} = 1.56$ mm starting from a breakdown plasma column having $T_{bd} = 45{,}000$ K and $d_{bd} = 80$ µm generated using $E_{bd} = 1.5$ mJ and $d_{gap} = 1$ mm. Instead, for the same parameters equation (2b) yields $d_{ig} = 2.77$ mm, a much larger value. This error stems from disregarding the fundamental contribution of the dissociation energy of highly ionized gases, the thermodynamic properties of which at chemical equilibrium can be computed using the CEA code as a function of temperature and pressure [31], as exemplified in Figure 1 for air at 1 bar. With these properties extracted for a range of pressures, it is then possible to solve the following equations:

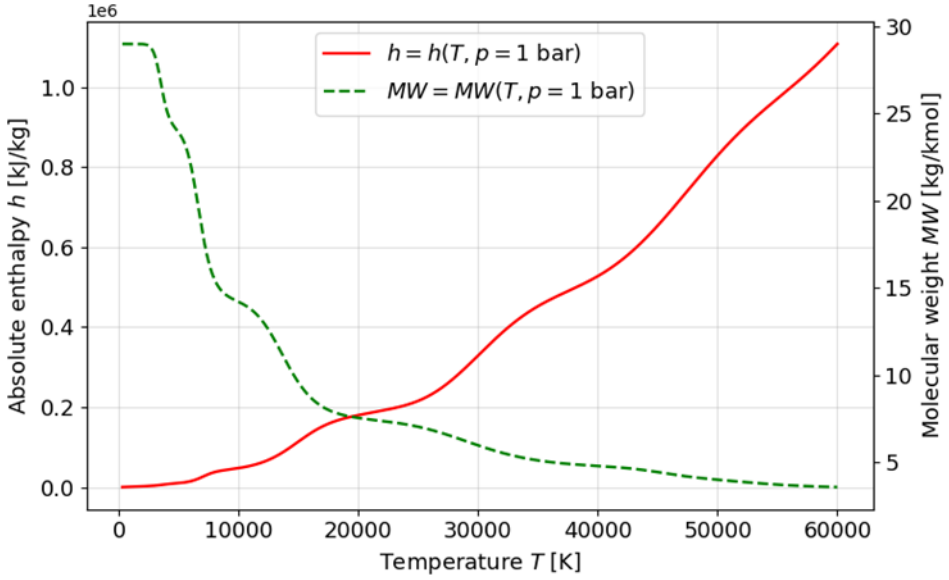

Figure 1. Absolute enthalpy and molecular weight of air at 1 bar as a function of temperature.

$$\begin{cases} m = \dfrac{p_u V_{bd} MW_u}{\mathcal{R} T_u} = \dfrac{p_{bd} V_{bd} MW_{bd}}{\mathcal{R} T_{bd}} = \dfrac{p_u V_{ig} MW_{ig}}{\mathcal{R} T_{ig}}, & \text{(4a)} \\ E_{bd} = m(u_{bd} - u_u) = m(h_{ig} - h_u). & \text{(4b)} \end{cases}$$

Equations (4a) and (4b) are respectively the proper mass and energy conservations for the expanding plasma column, which can be solved for a given T_{bd} yielding T_{ig} and $V_{ig} = \pi d_{gap}\, d_{ig}^2/4$. The results reported in Figure 2 show that, for $T_{bd} = 45{,}000$ K, $d_{bd} = 81$ µm and $d_{ig} = 1.59\, mm$, both within 2% of Sher's values [30], and that d_{ig} is only minimally affected by a variation of T_{bd}. Instead, T_{ig} remains much closer to the value yielded by equation (2a). The use of equations (4a) and (4b) in place of (2a) and (2b) is therefore highly recommended for plasma column expansions.

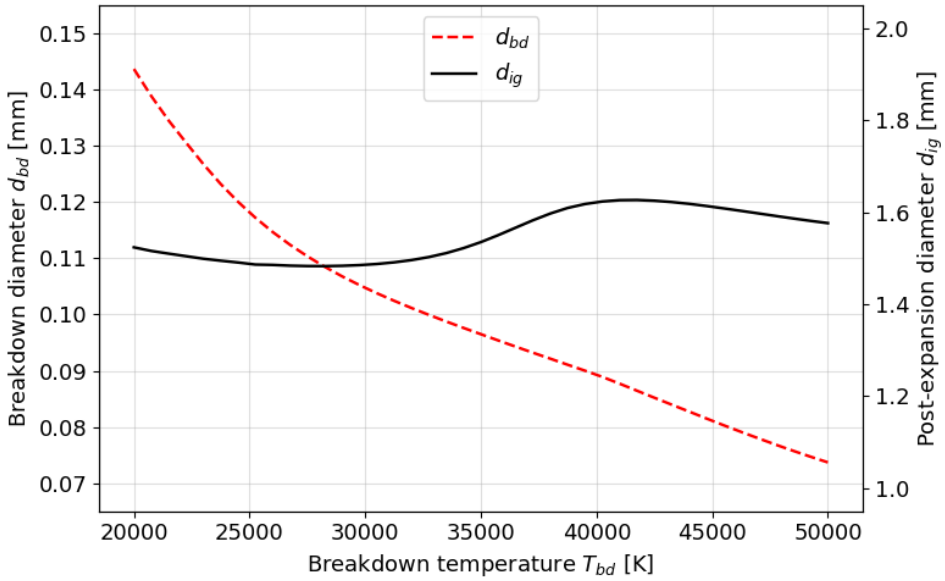

Figure 2. Breakdown (left) and post-expansion (right) plasma column diameters as a function of T_{bd}.

The second concern regards the key assumption of Sher's model, namely the expansion to p_u of a constant mass of plasma. The inconsistency of this assumption forces a '1D heat diffusion' phase that, disregarding both the heat of combustion and the mass flows near the electrodes, is abruptly terminated at the arbitrary value of $T_i = 3T_{adf}$. This was already noted by Ko et al. [29], who proposed a much more reasoned set of initial conditions based on previous solutions of cylindrical shockwave equations that allow for a mass increase in the activated plasma volume. This solution has been expanded on by Meyer and Wimmer [32] to include the use of air plasma properties for better estimating the post-cooldown temperature T_i, and it requires solving three relatively simple equations:

$$\begin{cases} r_{i,cyl} = 0.5 r_c = 0.5 \left(\dfrac{E_{bd}}{3.94 \pi d_{gap} p_u} \right)^{1/2}, & \text{(5a)} \\ t_i = 1.5 t_c = 1.5 \left(\dfrac{r_c}{\sqrt{\gamma_u p_u / \rho_u}} \right), & \text{(5b)} \\ (h_i - h_u) \rho_i V_i = \eta_{bd} E_{bd}. & \text{(5c)} \end{cases}$$

Equation (5a) gives the radius (i.e., volume) of the hot plasma cylinder, while equation (5b) provides the time it takes for the pressure to stabilize within 10% of p_u. Finally, equation (5c) is an open-boundary energy conservation that yields T_i, since $h_i = h_i(T_i)$ and $\rho_i = \rho_i(T_i)$ at $p_i \cong p_u$.

Using the present method and $\eta_{bd} \cong 1$ (see Section 3), for air at the same conditions as above the results are $r_{i,cyl} = 0.825$ mm, $t_i = 7.12$ μs, and $T_i = 6{,}139$ K, all of which fully consistent with heat diffusion models but stemming from a much sounder procedure. Moreover, this formulation can be extended to combustible mixtures through h_u, which is much higher than air's value at the same temperature and leads to $T_i \cong 6{,}800$ K for stoichiometric mixtures having $T_{adf} \in [2{,}200;\ 2{,}300]$ K. This value is very close to the $3T_{adf}$ cut-off reported in literature but reached via an arbitrary S_{plasma}. Finally, since the kernel is assumed to be spherical, $r_i = (3V_i/4\pi)^{1/3}$ is calculated and the (r_i, t_i, T_i) set constitutes the initial condition for the present kernel growth model.

2.2. The kernel growth model

As previously mentioned, the proposed kernel growth model is partially based on the expansion model for laminar flame kernels proposed by Ko et al. [29], which relies on the following assumptions:

- the flame kernel always retains a spherical shape;
- pressure is uniform and constant, equal to p_u;
- the ideal gas law holds true;
- the kernel contains burned mixture in chemical equilibrium at T_k;
- the combustion is represented by a one-step reaction controlled by deficient reactant A;
- the reaction zone has negligible thickness (due to large activation temperature $T_a \gg T_k$);
- unburned properties change with temperature, but $MW = const. = MW_u$.

Under these assumptions and after an extensive analysis of previous literature on thermo-diffusive flames, Ko and co-workers highlighted the existence of a 'stationary flame ball', which is a theoretical flame kernel that can exist indefinitely in a quiescent mixture due to a perfect balance between heat gained via combustion and heat lost via thermal diffusion towards the unburned mixture. This flame ball is named 'critical flame' and has critical temperature, T_{crt}, and radius, r_{crt}, expressed as follows:

$$\begin{cases} T_{crt} = T_u + \dfrac{1}{Le}\left(T_{adf} - T_u\right), & \text{(6a)} \\ r_{crt} = \dfrac{1}{Le}\dfrac{k_{crt}}{\rho_{crt} c_{p,crt}}\dfrac{T_{adf}}{T_{crt}} \cdot exp\left[\dfrac{T_a}{2}\left(\dfrac{1}{T_{crt}} - \dfrac{1}{T_{adf}}\right)\right]. & \text{(6b)} \end{cases}$$

According to Ko et al., the critical flame represents the threshold that a developing flame kernel must overcome to achieve successful ignition, which occurs only when the kernel grows beyond r_{crt} at temperature $T_k > T_{crt}$. However, the values of T_{crt} and r_{crt} depend primarily on Lewis number Le, which, although formally defined as the ratio between mixture heat diffusivity and mass diffusivity of the deficient reactant for a given fuel/air mixture, is actually a non-linear function of the equivalence ratio [14]. With growing Le, which leads to lower T_{crt} and higher r_{crt}, overcoming the critical condition becomes increasingly difficult, as the kernel tends to quench and extinguish before reaching r_{crt}. The main way to prevent this occurrence is providing additional energy, usually via an electric spark. This is the actual, heavily non-linear effect of flame stretch [15], the quantification of which requires dedicated kernel growth models.

A visualization of the proposed kernel growth model is provided in Figure 3. As the figure shows, the kernel is assumed to have uniform temperature T_k and mass fraction of deficient species (fuel or oxygen depending on ϕ) $Y_{A,k} = 0$. Moreover, the kernel does not border the unburned mixture, but rather the pre-heat zone of width δ_T and the reactant consumption zone of width δ_A (in general, $\delta_A \neq \delta_T$), beyond which the unburned values T_u and $Y_{A,u}$ are recovered. The kernel mass and energy conservation equations, with $[\cdot]_u(T_k) = [\cdot]_{u,k}$ for the sake of brevity, are:

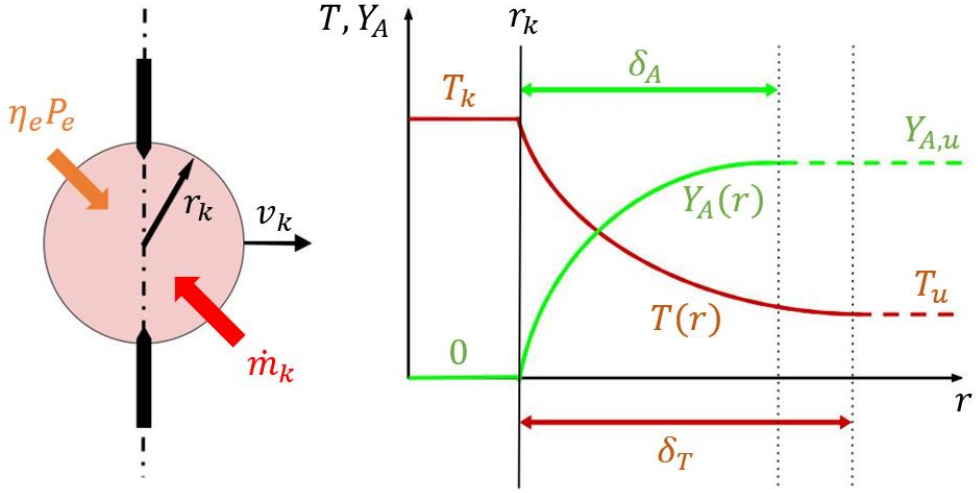

Figure 3. Kernel model (left) and temperature and deficient reactant profiles outside it (right).

$$\begin{cases} \dfrac{dm_k}{dt} = \dot{m}_k = \rho_u A_k S_{L,k}, & \text{(7a)} \\ \dfrac{dH_k}{dt} = \dot{m}_k h_{u,k} + \eta_e P_e - q_k A_k, \qquad q_k = q_k(\delta_T) = -k_{u,k} \left.\dfrac{\partial T}{\partial r}\right|_{r_k} & \text{(7b)} \end{cases}$$

Rearrangement of equation (7a) and, noting that $H_k = m_k h_k$ and $dh_k/dt = c_{p,k}\, dT_k/dt$, combination of equations (7a) and (7b) lead to the following pair of conservation equations:

$$\begin{cases} \rho_k A_k \dfrac{dr_k}{dt} = \dot{m}_k + \dfrac{m_k}{T_k}\dfrac{dT_k}{dt}, & \text{(8a)} \\ m_k c_{p,k} \dfrac{dT_k}{dt} = \dot{m}_k \left(h_{u,k} - h_k\right) + \eta_e P_e - q_k A_k. & \text{(8b)} \end{cases}$$

In particular, equation (8b) indicates that the kernel temperature rises due to P_e, if supplied, and to the heat of reaction calculated at T_k, while it falls due to the conductive losses $q_k A_k$. However, q_k is unknown, as it depends on δ_T. To find it, the assumption made by Ko et al. [29] of parabolic profiles for $T(r)$ and $Y_A(r)$ within δ_T and δ_A, respectively, is retained, resulting in:

$$\begin{cases} T(r) = T_u + (T_k - T_u)\left[\dfrac{(r_k + \delta_T) - r}{\delta_T}\right]^2, \quad r \in [r_k;\, r_k + \delta_T], & \text{(9a)} \\ Y_A(r) = Y_{A,u}\left\{1 - \left[\dfrac{(r_k + \delta_A) - r}{\delta_A}\right]^2\right\}, \quad r \in [r_k;\, r_k + \delta_A]. & \text{(9b)} \end{cases}$$

Equation (9b) is used to find δ_A by equating the $\dot{m}_k^A$ entering the kernel via mass diffusion to the $\dot{m}_k^A$ transported via convection:

$$\dot{m}_k^A = \rho_{u,k} A_k \mathcal{D}_{A,k} \left.\frac{\partial Y_A}{\partial r}\right|_{r_k} = \rho_{u,k} A_k \mathcal{D}_{A,k} \frac{2Y_{A,u}}{\delta_A} = Y_{A,u} \dot{m}_k = Y_{A,u} \rho_u A_k S_{L,k}, \qquad (10)$$

which, assuming that Le is defined at T_k, i.e., $Le = k_{u,k}/(\rho_{u,k} c_{p,u,k} \mathcal{D}_{A,k})$, yields an expression for δ_A:

$$\delta_A = \frac{2}{Le} \frac{k_{u,k}}{c_{p,u,k}} \frac{1}{\rho_u S_{L,k}}. \qquad (11)$$

To find $\dot{m}_k$ and δ_A, defining the behavior of $S_{L,k} = S_L(T_k \neq T_{adf})$ becomes necessary. This is done by using an expression similar to the one used by Ko et al. [29], which is

$$S_{L,k} = S_{L,adf}\left(\frac{\alpha_k}{\alpha_{adf}}\right)^n exp\left[-\frac{T_a}{2}\left(\frac{1}{T_k}-\frac{1}{T_{adf}}\right)\right], \tag{12}$$

where the power-law term accounts for the altered heat diffusion, as well as mass diffusion at fixed Le, while the exponential term represents the altered speed of a one-step combustion reaction with activation temperature T_a. Exponent n is set as follows:

$$\begin{cases} n = 1 & if\ r_k/r_{crt} < 1, \quad (13a) \\ n = 2 - r_k/r_{crt} & if\ r_k/r_{crt} \in [1;\ 1.5], \quad (13b) \\ n = 0.5 & if\ r_k/r_{crt} > 1.5. \quad (13c) \end{cases}$$

Expressions (13a) and (13c) are consistent with the critical and planar flame, respectively, while (13b) is a linear averaging that prevents the sharp cut-off at $r_k/r_{crt} = 1.5$ imposed by Ko and co-workers.

Determination of δ_A is a requirement for calculating δ_T, which is achieved by writing the deficient reactant and energy conservations outside the kernel, where no reaction occurs, in the thermo-diffusive framework of no convection and constant density [18] [29]. These conservation laws are:

$$\begin{cases} \rho\dfrac{\partial Y_A}{\partial t} = \dfrac{1}{r^2}\dfrac{\partial}{\partial r}\left(r^2\rho\mathcal{D}_A\dfrac{\partial Y_A}{\partial r}\right), & (14a) \\ \rho\dfrac{\partial h}{\partial t} = \dfrac{1}{r^2}\dfrac{\partial}{\partial r}\left(r^2 k\dfrac{\partial T}{\partial r}\right). & (14b) \end{cases}$$

Specialization of equations (14a) and (14b) at r_k using the parabolic profiles of (9a) and (9b) gives:

$$\begin{cases} v_{k,tdiff} = \mathcal{D}_{A,k}\left(\dfrac{1}{\delta_A}-\dfrac{2}{r_k}\right), & (15a) \\ \dfrac{dT_k}{dt} + v_{k,tdiff}\dfrac{2(T_k-T_u)}{\delta_T} = \dfrac{2(T_k-T_u)}{\delta_T}\dfrac{k_{u,k}}{\rho_{u,k}c_{p,u,k}}\left(\dfrac{1}{\delta_T}-\dfrac{2}{r_k}\right), & (15b) \end{cases}$$

where $v_{k,tdiff}$ is a 'thermo-diffusive dr_k/dt' that does not coincide with the actual kernel expansion speed $v_k = dr_k/dt$. In fact, $v_{k,tdiff}$ is shared among the two equations, and can be made to disappear via substitution leading to a single expression linking dT_k/dt with δ_T. Combining this expression with equation (8b) enables retrieving a simple algebraic equation for δ_T:

$$C_2{\delta_T}^2 + C_1\delta_T + C_0 = 0, \tag{16}$$

the coefficients of which are as follows:

$$\begin{cases} C_0 = -2(T_k-T_u)\dfrac{k_{u,k}}{\rho_{u,k}C_{p,u,k}}, & (17a) \\ C_1 = -C_0\left[\dfrac{1}{Le\,\delta_A}+\left(1-\dfrac{1}{Le}\right)\dfrac{2}{r_k}\right] - 2(T_k-T_u)\dfrac{A_k}{m_k c_{p,k}}, & (17b) \\ C_2 = \dfrac{\dot{m}_k\left(h_{u,k}-h_k\right)+\eta_e P_e}{m_k C_{p,k}}. & (17c) \end{cases}$$

Equations (8a), (8b), (11), and (16) constitute a linear system of four equations, whose unknowns are T_k, r_k, δ_A, and δ_T. The solution can be advanced in time using a simple explicit numerical method.

As mentioned, many elements of the present model were taken from Ko and co-workers [29], but a key difference between the two models is that the latter does not assume that $\dot{m}_k = \rho_u A_k S_{L,k}$. Instead, it treats $\dot{m}_k$ as a parameter to be eliminated by integrating the mass and energy conservation equations in the pre-heat zone $[r_k;\ r_k+\delta_T]$ to retrieve dr_k/dt. However, this operation is very complex, and the mathematical steps that lead to the final equation are quite cryptic, ultimately preventing the model reproducibility. On the contrary, here we immediately assign to $S_{L,k}$ both a diffusive meaning ($S_{L,k} \propto 1/\delta_A$) and a convective one ($S_{L,k} \propto \dot{m}_k$), giving T_k a much more important role in driving the kernel

evolution. This approximation leads to a much simpler growth model, the prediction capabilities of which will be assessed in Section 3. Finally, notable additional differences from Ko et al.'s model are:

- use of absolute enthalpy;
- different properties between burned (kernel) and unburned gases (e.g., $MW_k \neq MW_u$);
- no use of an arbitrary 'entrainment mass flow' $\propto P_e$ around the electrodes.

2.3. Quantification of turbulence effects on kernel development

The application of any kernel growth model in SI engines cannot disregard the effects of turbulence on the flame kernel development. However, the present model is formulated for laminar conditions, and therefore a strategy is required to include turbulence into the present framework. Remembering that turbulence tends to wrinkle or corrugate the developing flame front with increasing intensity as the kernel grows experiencing all length scales [33], two mutually exclusive solutions appear promising. The first one assumes that turbulence increases the flame front area while maintaining an overall spherical kernel ($V_k = 4/3\pi r_k^3$) and a laminar flame speed, i.e.,

$$A_{k,T} = \mathcal{F}_A(u') \cdot A_k = \mathcal{F}_A(u') \cdot 4\pi r_k^2, \tag{18}$$

whereas the second one assumes that turbulence affects the flame speed with 'laminar' area, i.e.,

$$S_{T,k} = \mathcal{F}_S(u') \cdot S_{L,k}. \tag{19}$$

Equation (18) is typical of fractal turbulence models [33], with $\mathcal{F}_A(u') \geq 1$ being the 'wrinkling factor', whereas equation (19) is employed by the BML model [4] and $\mathcal{F}_S(u') \geq 1$ takes the meaning of an 'acceleration factor'. Both options are viable for the proposed kernel growth model.

3. Results and discussion

In this section both qualitative and quantitative analysis are conducted to examine the response of the present model to a variety of conditions. All unburned properties were computed using Cantera [34] and GRI-Mech 3.0 [35], while burned properties were extracted in-house using the CEA tool [31]. The breakdown efficiency is set at $\eta_{bd} = 0.94$ following Maly's indication [2].

3.1. Qualitative behavior of the proposed model

The first analysis regards the expected behavior of the proposed kernel growth model, and focus is put on the effect of a variable Lewis number, which is the parameter that most affects the kernel development. To do so, a reference fuel/air mixture is ignited in atmospheric conditions using $E_{bd} = 1$ mJ and $d_{gap} = 1$ mm, being $S_{L,adf} = 0.3$ m/s, $T_{adf} = 2{,}000$ K, $T_a = 20{,}000$ K, $v_{k,adf} = 2$ m/s. No P_e is supplied, while Le is varied arbitrarily between five values.

The result of this simulation is shown in Figure 4. As expected, immediately after the breakdown the kernel cools down regardless of Le as the heat of reaction supersedes electricity as the primary energy source. However, while for $Le = 1$ the kernel immediately reaches adiabatic flame conditions, this is not true for the other cases. In particular, the $Le = 0.6$ kernel remains super-adiabatic for a much longer time, positively affecting the expansion and resulting in a notably larger final r_k. On the contrary, all $Le > 1$ kernels experience a measurable cooldown and consequent slowdown caused by the high flame curvature, which enhances the heat loss towards the unburned gas. This is most evident around the critical radius, but if the kernel grows beyond r_{crt} it reaccelerates, ultimately reaching the adiabatic condition, albeit with a much smaller final radius. Instead, in the $Le = 2.2$ case r_{crt} is too large (about 17 mm) and the kernel quenches, with v_k dropping to zero. Similar values of Le are typical for many hydrocarbon/air mixtures [16], which is why in real-world applications such as SI engines successful ignition is achieved by supporting the growing kernel with electric energy (i.e. $P_e > 0$) supplied via the spark plugs. Finally, note that, regardless of any flame initiation, for adiabatic planar flames Le is expected to equal the ratio between thermal thickness and mass diffusion thickness [19]. This result is recovered in this model, as the δ_T/δ_A ratio of Figure 4(d) effectively tends to Le if the kernel does not extinguish.

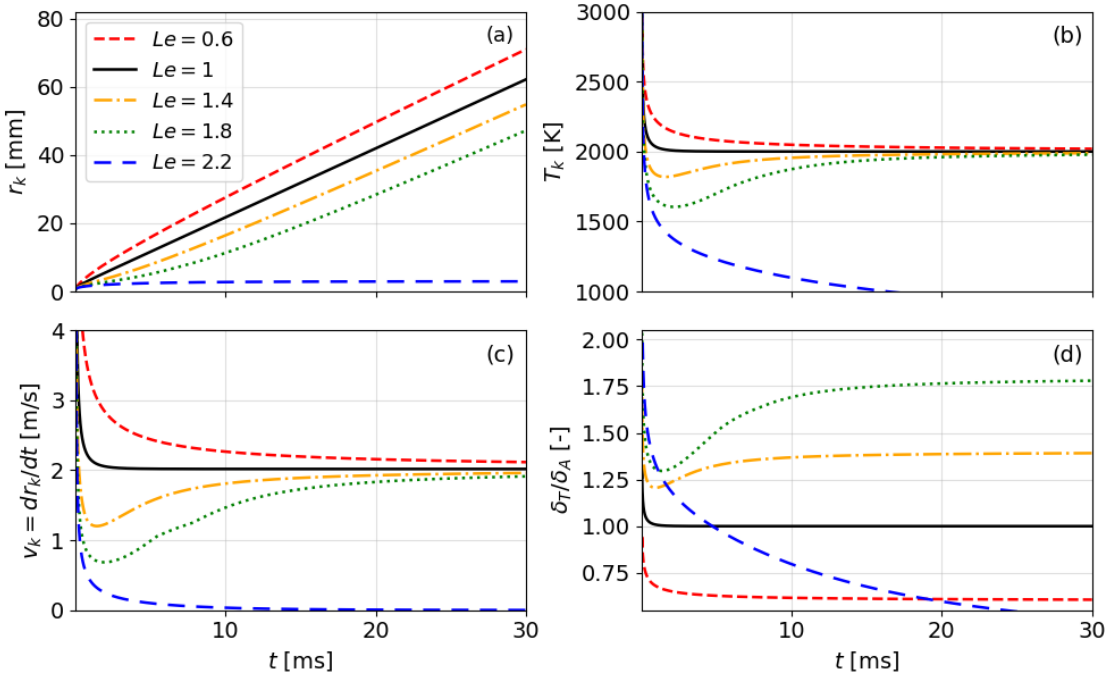

Figure 4. Kernel radius (a), temperature (b), expansion speed (c) and thickness ratio (d) at varying Le.

3.2. Laminar kernel expansion

Concerning the flame kernel development in laminar conditions, the predictions obtained with the proposed model are compared with the experiments [28] and model results [29] presented by Ko and co-workers for atmospheric lean propane/air flames. Three equivalence ratios, each with two different electric energy supplies, are examined. The power supply $P_{eff}(t) = \eta_e(t)P_e(t)$ is set according to the provided sub-model, while E_{bd} is set within the range mentioned [28] and all other modelling parameters are taken from literature. The full list of parameters is reported in Table 1, where for each ϕ the smaller value ($E_{e,1}$) always leads to kernel extinction, while the larger one ($E_{e,2}$), slightly above the minimum ignition energy, is the value used in the experiments. $E_{e,2}$ often led to a successful ignition, but failures were also observed due to stochastic variations in the test chamber.

Table 1. Parameters used for the modelling of the laminar propane/air kernels of Subsection 3.2

$\boldsymbol{\phi}$ [−]	$S_{L,adf}$ [m/s] [36]	Le [−] [14]	T_a [K] [14]	E_{bd} [mJ]	d_{gap} [mm]	$E_{e,1}$ [mJ]	$E_{e,2}$ [mJ]	t_e [ms]
0.8	0.277	1.57	22,000	0.5	1.0	1.7	3.6	0.56
0.7	0.201	1.62	20,000	1.0	2.0	2.0	3.0	0.56
0.6	0.130	1.68	18,000	1.0	2.0	44.0	61.0	3.55

The comparison between present predictions, experimental data, and literature model results is shown in Figure 5. The present model appears clearly capable of reconstructing the different kernel expansion trends, but careful observation of the results highlights some discrepancies that warrant a deeper analysis. For the richest mixture ($\phi = 0.8$) in Figure 5(a), this model captures very well the successful ignition, but the simulation with lower energy still conducts to an ignition, albeit with an extremely slow expansion speed. Instead, the slightly leaner mixture ($\phi = 0.7$) in Figure 5(b) appears

as the most challenging prediction, reporting a moderate underestimation of the expansion speed for the ignition case, especially when $r_k/r_{crt} \cong 2$, coupled with a limited overestimation for the non-ignition one. On the other hand, the best prediction is obtained for the leanest mixture ($\phi = 0.6$) in Figure 5(c), where the successful ignition is captured with just a minor underestimation, while the unsuccessful ignition is clearly below any high-energy experimental data point and on par with Ko et al.'s model. However, due to the different thermophysical mixture properties r_{crt} is smaller than Ko's estimate, thus facilitating the expansion acceleration.

Following this analysis, it appears that the present kernel expansion model is slightly less responsive than Ko and co-workers' one, tending to overestimate the probability of a kernel survival while often underestimating the kernel growth after a successful ignition. This outcome is likely caused by the assumption of $S_{L,k} \propto \dot{m}_k$, which may not be true when the flame front curvature is very high and will be subject to future investigation. However, this choice makes the model much simpler, and has also the advantage of removing any need for an S_{plasma} related to arbitrary heat diffusion processes. Some mispredictions are observed, but they are expected to be of limited importance for the turbulent flames typical of SI engines.

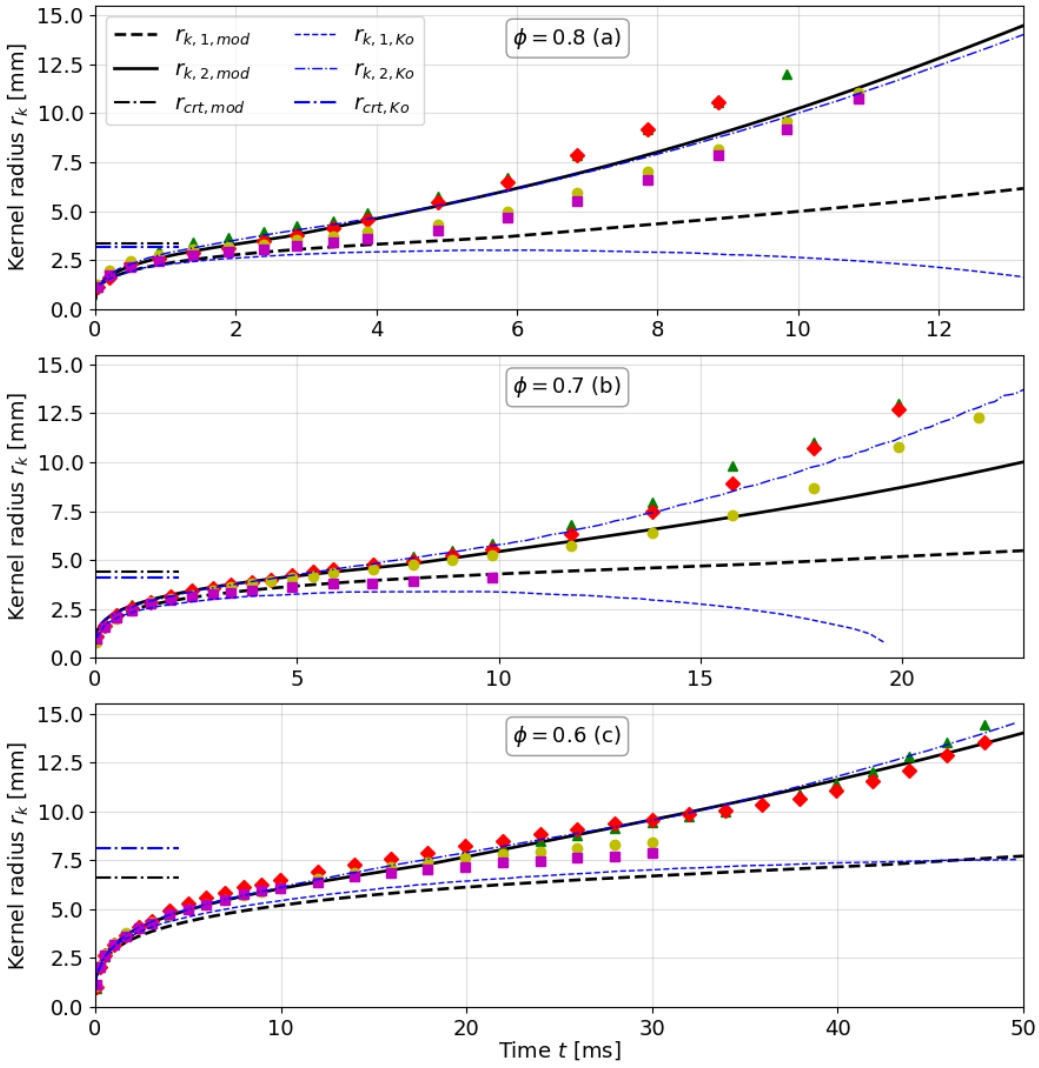

Figure 5. Comparison between present model predictions (mod), Ko and co-workers' predictions (Ko), and their experiments (scatter plots). Subscripts (1,2) refer to the E_e values of Table 1.

3.3. Turbulent kernel expansion

As anticipated, the present kernel expansion model is now tested in the turbulent conditions of the propane-powered SI engine examined and discussed by Herweg and Maly [4]. In this case we limit the comparison to the central spark case, since the peripheral case affects only the turbulence intensity defined via the BML model, which is not subject to discussion. Coherently, turbulence is interpreted according to equation (19) and $\mathcal{F}_S(u')$ is computed using $S_L = S_{L,adf}$ as done by Herweg and Maly:

$$\mathcal{F}_S(u') = 1 + \left(\frac{u'}{u' + S_L}\right)^{\frac{1}{2}} \left[1 - exp\left(-\frac{r_k}{L}\right)\right]^{\frac{1}{2}} \left[1 - exp\left(-\frac{t}{t_0}\right)\right]^{\frac{1}{2}} \frac{u'}{S_L} \left[1 + \frac{4.4}{1 + 3.919(u'/S_L)}\right]^{1/2}, \quad (20)$$

with $t_0 = L/(u' + S_L)$. Note that the I_0 defined by equation (3) that normally appears in this equation is set to 1, as the present model assumes that flame stretch is accounted for within $S_{L,k}$. Moreover, for brevity the comparison is limited to the TCI (transistorized coil ignition) case. The relevant modelling parameters are listed in Table 2, where E_{bd}, not specified in the paper, is chosen so that $r_k \cong 0.5$ mm after 10 ms as shown by the experiments. The $u' = u'(\text{rpm})$ values are the same as reported [4].

Table 2. Relevant parameters used for the modelling of turbulent propane/air kernels of Subsection 3.3. $p_u = 5\ bar$, all other unlisted parameters are the same as reported [4].

$\boldsymbol{\lambda = \phi^{-1}}$ [−]	$S_{L,adf}$ [m/s]	Le [−] [14]	T_a [K] [14]	E_{bd} [mJ]	d_{gap} [mm]	E_e [mJ]	$t_e(u')$ [ms]
1	0.95	1.30	28,000	0.5	1.0	60	1.1 to 1.7
1.3	0.59	1.59	22,000	0.5	1.0	60	1.1 to 1.7
1.5	0.41	1.64	21,000	0.5	1.0	60	1.1 to 1.7

The comparison with the experimental data is shown in Figure 6, and it appears quite satisfying. Firstly, in all these cases r_{crt} calculated with equation (6b) is less than 0.5 mm due to the high T_{adf} values resulting from the mixture compression in the cylinder, causing the initial expansion to be controlled by $S_L(T_k \geq T_{adf})$. The proposed model is able to capture very well this initial fast expansion at $r_k < 1$ mm, as well as the drop in v_k around $r_k \cong 1$ mm and $t \cong 150$ ms. Then, around the same instant the plots for different rotational speeds start diverging due to the different turbulence intensities, and the resulting kernel expansion accelerations are recovered with good accuracy for all equivalence ratios and turbulence intensities. The few notable differences mainly regard the slowdown overestimation at $t \in [100;\ 300]$ ms and $r_k \in [1;\ 1.5]$ mm, which may be related to the simplified model used for the energy transfer efficiency [4], and limited misestimations in a few of the turbulence-controlled expansion speeds, such as for the $\lambda = 1$ and 300 rpm case in Figure 6(a) and (b), which are likely to derive from approximations in the BML model.

A similar comparison is then conducted in Figure 7 against Herweg and Maly's model results. While the overall kernel expansion trends are very similar, two main differences are worth noting. Firstly, their model appears to misestimate the kernel growth when $r_k < 1$ mm especially for the richer mixtures, as shown by Figure 7(b), (d), and (f). Since their maximum v_k is around 10 m/s, this misprediction is most likely due to the use of S_{plasma}, which seems unable to fully capture the breakdown effect. Secondly, their model consistently overestimates the kernel growth at larger values of r_k and t compared to both the present model and the experimental data. In this case, the reason lies in the I_0 calculated via equation (3), which roughly scales with $(1 - Le)v_k/r_k$ and yields very small or negative values for $r_k < 2$ mm and $Le > 1$. The only way to avoid this is setting $Le = 1$ as done by Herweg and Maly [4], but this causes I_0 to be overestimated for larger r_k, ultimately resulting in the observed overestimation of v_k.

To summarize, from the comparisons discussed in this section it appears that the kernel expansion model proposed in this paper not only is reasonably accurate for laminar flames, but it is also capable of satisfying kernel growth predictions in the moderately turbulent conditions typical of SI engines.

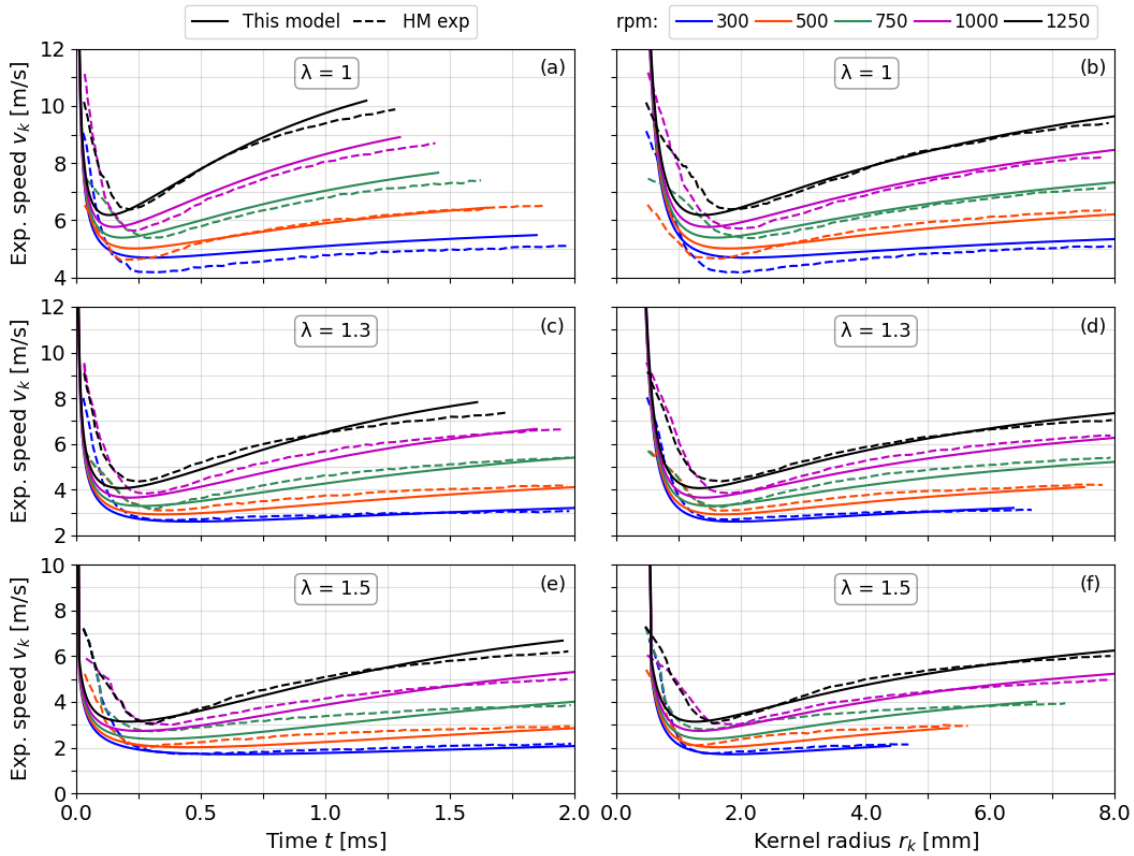

Figure 6. Comparison between present predictions and experimental data from Herweg and Maly (HM exp). Kernel expansion speed plotted against time in (a), (c), (e), and radius in (b), (d), (f). Increasing rpm values [rev/min] are associated with increasing turbulence intensities [4].

A final note is made regarding the possibility of a non-zero mean flow velocity, which can occur especially for off-center spark plugs [4]. In such a case the kernel would be transported by the convective flow and the discharge itself would experience a U-shaped distortion that may lead to a restrike event, albeit at a voltage typically lower than that of the initial breakdown [11] [12]. Although the present model currently cannot account for this effect, an amendment could be made to include a restrike, which could be made to happen as soon as the distance between kernel and spark plug centers is larger than r_k, and the higher temperature would indeed result in a lower voltage. However, multiple flame kernels would require tracking, which implies a need for deep model modifications.

4. Conclusions and future developments

Flame kernel initiation is SI engines has been a topic of interest for a long time, but the majority of available phenomenological kernel growth models are based on simplifying assumptions that limit their accuracy, whereas numerical simulations have a high computational cost. With the aim of achieving higher accuracy in a phenomenological framework, this paper has presented a flame kernel development model that, starting from the near-breakdown plasma column, describes the early kernel growth considering temperature and deficient reactant profiles outside the flame kernel. The initial conditions derive from quantification of the post-breakdown shockwave effects, while the model formulation enables inherent consideration of flame stretch effects without using linear relations unsuited to the high flame front curvature. While the proposed model uses some elements from Ko et al. [29], work has been conducted to obtained a clearer, easier, replicable kernel growth model that can also include turbulence effects, which are key for proper modelling of SI engines.

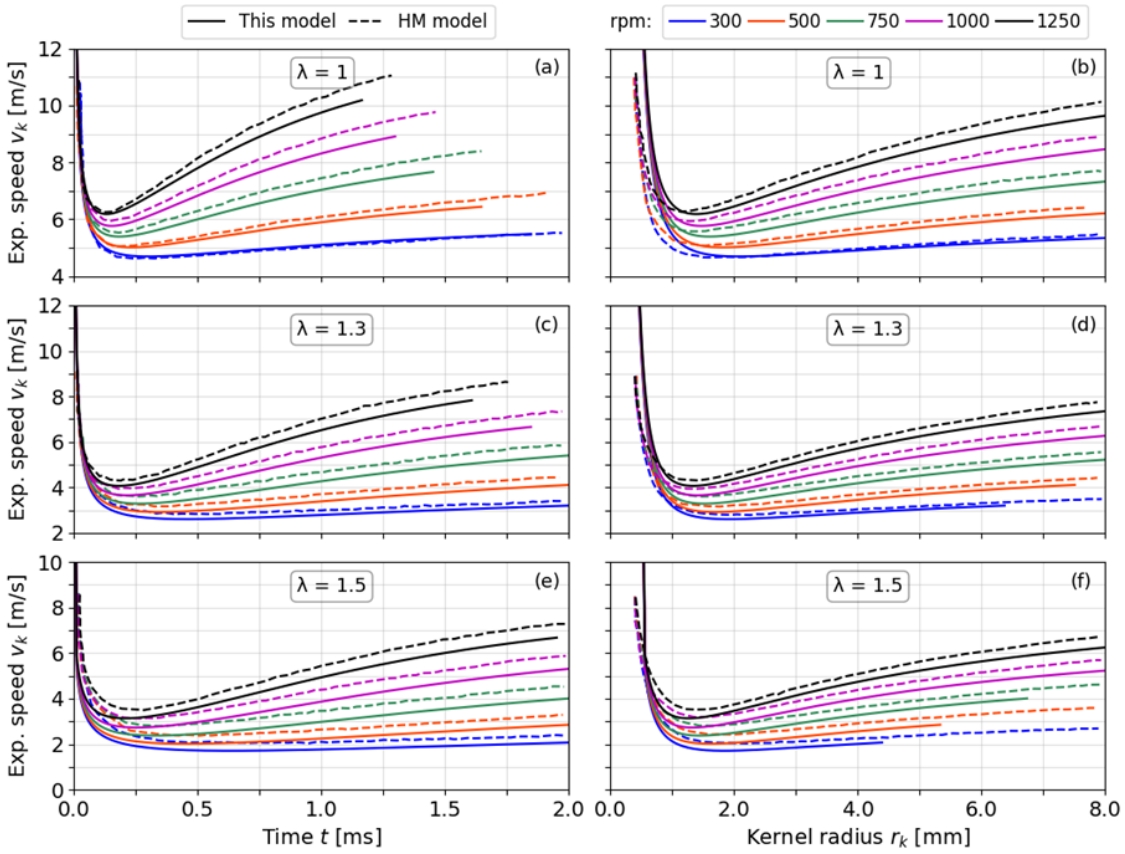

Figure 7. Comparison between present predictions and model results from Herweg and Maly (HM model). Kernel expansion speed plotted against time in (a), (c), (e), and radius in (b), (d), (f). Increasing rpm values [rev/min] are associated with increasing turbulence intensities [4].

Results have been presented for three cases. In the first one, an analysis of the model response as a function of the Lewis number has been conducted to highlight its effect on the kernel growth, which is increasingly hindered as Le rises, possibly leading even to flame extinction. Then, the present growth predictions have been compared with Ko and co-workers' experimental and modelling data on laminar flame kernels [31], showing acceptable results but also some mispredictions for all cases. Finally, a second comparison has been conducted against Herweg and Maly's experiments and predictions on turbulent flame kernels in an SI engine [4], where the present model has shown a good match with the experimental data across all sub-cases without any need for linear flame stretch models. This outcome is key, because it indicates that this model is suitable for use in the simulation of SI engines.

Future developments will proceed in two directions. Firstly, work will be conducted on implementing this model into full SI engine combustion models, and an effect is expected for the low-load and low-turbulence conditions in which failure of linear stretch models is observed [27]. This will require the non-trivial extraction of properties (e.g., Le, T_a) of complex fuel blends at variable temperatures and pressures, but this can be done according to literature techniques [14]. Secondly, simplifying assumptions such as $S_{L,k} \propto \dot{m}_k$ or the use of parabolic profiles are likely to be the source of the misestimations reported in Subsection 3.2, suggesting that the kernel model itself should undergo further development. In this regard, the rigorous analysis of thermo-diffusive flames [19] appears promising, but it needs adapting to the convective framework of variable-density combustion.

Acknowledgements
This work was supported by the co-financing of the European Union - FSE-REACT-EU, PON Research and Innovation 2014-2020 DM 1062/2021.

Nomenclature

Acronyms		T	Temperature
BML	Bray-Moss-Libby	u	Absolute specific internal energy
CEA	Chemical Equilibrium Applications	u'	Turbulence intensity
CFD	Computational Fluid Dynamics	v	Expansion velocity
ICE	Internal Combustion Engine	V	Volume
SI	Spark Ignition	Y	Mass fraction
Symbols		α	Thermal diffusivity
A	Area or deficient reactant	γ	Specific heat ratio
c_p	Isobaric mass heat capacity	δ	Diffusion or flame thickness
d, d_{gap}	Diameter, electrode gap distance	η	Energy deposition efficiency
$\mathcal{D}$	Mass diffusivity	ϕ, λ	Equivalence and dilution ratio
E	Electric energy	ρ	Density
h, H	Absolute (specific) enthalpy	*Subscripts*	
I_0	Linear stretch factor	$[\cdot]_a$	Activation
k	Thermal conductivity	$[\cdot]_A$	Deficient reactant
L	Turbulence integral length scale	$[\cdot]_{adf}$	Adiabatic flame
Le	Lewis number	$[\cdot]_{bd}$	Breakdown
$m, \dot{m}$	Mass, mass flow	$[\cdot]_{crt}$	Critical
MW	Molecular weight	$[\cdot]_{cyl}$	Cylindrical
p	Pressure	$[\cdot]_e$	Electric
P	Electric power	$[\cdot]_i$	Initial condition
q	Heating power per unit area	$[\cdot]_{ig}$	Ignition
r	Radius, radial distance	$[\cdot]_k$	Kernel
S	Relative flame speed	$[\cdot]_L$	Laminar
t, t_0	Time, turbulence integral time scale	$[\cdot]_u$	Unburned

References

[1] M. N. Plooster, "Numerical Simulation of Spark Discharges in Air," *Physics of Fluids,* vol. 14, no. 10, pp. 2111-2123, 1971.

[2] R. Maly and M. Vogel, "Initiation and propagation of flame fronts in lean CH4-air mixtures by the three modes of the ignition spark," in *Symposium (international) on combustion*, 1979.

[3] R. Maly, "Spark ignition: its physics and effect on the internal combustion engine," in *Fuel economy: In road vehicles powered by spark ignition engines*, Springer, 1984, pp. 91-148.

[4] R. Herweg and R. Maly, "A fundamental model for flame kernel formation in SI engines," *SAE transactions,* pp. 1947-1976, 1992.

[5] Z. Tan and R. D. Reitz, "An ignition and combustion model based on the level-set method for spark ignition engine multidimensional modeling," *Combustion and Flame,* vol. 145, no. 2, pp. 1-15, 2006.

[6] H. Shen, P. C. Hinze and J. B. Heywood, "A study of cycle-to-cycle variations in SI engines using a modified quasi-dimensional model," *SAE transactions,* pp. 1573-1582, 1996.

[7] S. Refael and E. Sher, "A theoretical study of the ignition of a reactive medium by means of an electrical discharge," *Combustion and Flame,* vol. 59, no. 1, pp. 17-30, 1985.

[8] J. Song and M. Sunwoo, "Flame kernel formation and propagation modelling in spark ignition engines," *Proceedings of the Institution of Mechanical Engineers, Part D: Journal of Automobile*

Engineering, vol. 215, no. 1, pp. 105-114, 2001.

[9] B. L. Salvi and K. A. Subramanian, "Experimental investigation and phenomenological model development of flame kernel growth rate in a gasoline fuelled spark ignition engine," *Applied energy,* vol. 139, pp. 93-103, 2015.

[10] S. Falfari and G. M. Bianchi, "Development of an ignition model for SI engines simulation," *SAE technical paper,* 2007.

[11] T. Lucchini, L. Cornolti, G. Montenegro, G. D'Errico, M. Fiocco, A. Teraji and T. Shiraishi, "A comprehensive model to predict the initial stage of combustion in SI engines," *SAE technical paper,* 2013.

[12] L. Sforza, T. Lucchini, A. Onorati, X. Zhu and S. Y. Lee, "Experimental and numerical study of flame kernel formation processes of propane-air mixture in a pressurized combustion vessel," *SAE technical paper,* 2017.

[13] M. Thiele, J. Warnatz and U. Maas, "Geometrical study of spark ignition in two dimensions.," *Combustion Theory and Modelling,* vol. 4, no. 4, pp. 413-434, 2000.

[14] C. J. Sun, C. J. Sung, L. He and C. K. Law, "Dynamics of weakly stretched flames: quantitative description and extraction of global flame parameters," *Combustion and Flame,* vol. 1, no. 2, pp. 108-128, 1999.

[15] C. J. Sun and C. K. Law, "On the nonlinear response of stretched premixed flames," *Combustion and Flame,* vol. 121, no. 1-2, pp. 236-248, 2000.

[16] A. P. Kelley and C. K. Law, "Nonlinear effects in the extraction of laminar flame speeds from expanding spherical flames," *Combustion and Flame,* vol. 156, no. 9, pp. 1844-1851, 2009.

[17] A. P. Kelley, G. Jomaas and C. K. Law, "Critical radius for sustained propagation of spark-ignited spherical flames," *Combustion and Flame,* vol. 156, no. 5, pp. 1006-1013, 2009.

[18] M. Champion, B. Deshaies and G. Joulin, "Relative influences of convective and diffusive transports during spherical flame initiation," *Combustion and Flame,* vol. 74, no. 2, pp. 161-170, 1988.

[19] Z. Chen and Y. Ju, "Theoretical analysis of the evolution from ignition kernel to flame ball and planar flame," *Combustion Theory and Modelling,* vol. 11, no. 3, pp. 427-453, 2007.

[20] C. F. Gouldin, "An application of fractals to modeling premixed turbulent flames," *Combustion and Flame,* vol. 68, no. 3, pp. 249-266, 1987.

[21] N. Chakraborty, M. Klein and R. S. Cant, "Stretch rate effects on displacement speed in turbulent premixed flame kernels in the thin reaction zones regime," *Proceeding of the Combustion Institute,* vol. 31, no. 1, pp. 1385-1392, 2007.

[22] M. Reyes, F. V. Tinaut, B. Giménez and A. Pérez, "Characterization of cycle-to-cycle variations in a natural gas spark ignition engine," *Fuel,* vol. 140, pp. 752-761, 2015.

[23] C. Forte, E. Corti, G. M. Bianchi, S. Falfari and S. Fantoni, "A RANS CFD 3D methodology for the evaluation of the effects of cycle by cycle variation on knock tendency of a high performance spark ignition engine," *SAE technical paper,* 2014.

[24] S. Demesoukas, P. Brequigny, C. Caillol, F. Halter and C. Mounaïm-Rousselle, "0D modeling aspects of flame stretch in spark ignition engines and comparison with experimental results," *Applied Energy,* vol. 179, pp. 401-412, 2016.

[25] L. Teodosio, F. Bozza, D. Tufano, P. Giannattasio, E. Distaso and R. Amirante, "Impact of the laminar flame speed correlation on the results of a quasi-dimensional combustion model for Spark-Ignition engine," *Energy Procedia,* vol. 148, pp. 631-638, 2018.

[26] F. Bozza, V. De Bellis, P. Giannattasio, L. Teodosio and L. Marchitto, "Extension and validation of a 1D model applied to the analysis of a water injected turbocharged spark ignited engine at high loads and over a WLTP driving cycle," *SAE International Journal of Engines,* vol. 10, no. 4,

pp. 2141-2153, 2017.

[27] V. De Bellis, E. Malfi, L. Teodosio, P. Giannattasio and F. Di Lenarda, "A novel laminar flame speed correlation for the refinement of the flame front description in a phenomenological combustion model for spark-ignition engines.," *SAE International Journal of Engines,* vol. 12, no. 3, pp. 251-270, 2019.

[28] Y. Ko, R. W. Anderson and V. S. Arpaci, "Spark Ignition of Propane-Air Mixtures Near the Minimum Ignition Energy: Part I. An Experimental Study," *Combustion and Flame,* vol. 83, no. 1-2, pp. 75-87, 1991.

[29] Y. Ko, V. S. Arpaci and R. W. Anderson, "Spark ignition of propane-air mixtures near the minimum ignition energy: Part II. A model development," *Combustion and Flame,* vol. 83, no. 1-2, pp. 88-105, 1991.

[30] E. Sher, J. Ben-Ya'ish and T. Kravchik, "On the birth of spark channels," *Combustion and Flame,* vol. 89, no. 2, pp. 186-194, 1992.

[31] B. J. McBride, Computer program for calculation of complex chemical equilibrium compositions and applications, Cleveland, OH: NASA Glenn Research Center, 1996.

[32] G. Meyer and A. Wimmer, "A thermodynamic model for the plasma kernel volume and temperature resulting from spark discharge at high pressures," *Journal of Thermal Analysis and Calorimetry,* vol. 133, no. 2, pp. 1195-1205, 2018.

[33] V. De Bellis, F. Bozza and D. Tufano, "A comparison between two phenomenological combustion models applied to different SI engines," *SAE Technical Paper,* 2017.

[34] D. G. Goodwin, H. K. Moffat, S. I., S. R. L. and B. W. Weber, "Cantera: An Object-oriented Software Toolkit for Chemical Kinetics, Thermodynamics, and Transport Processes," Version 2.5, 2021. [Online]. Available: https://www.cantera.org.

[35] G. P. Smith, “GRI-Mech 3.0,” [Online]. Available: http://combustion.berkeley.edu/gri-mech/.

[36] R. Amirante, E. Distaso, P. Tamburrano and R. D. Reitz, "Laminar flame speed correlations for methane, ethane, propane and their mixtures, and natural gas and gasoline for spark-ignition engine simulations," *International Journal of Engine Research,* vol. 18, no. 9, pp. 951-970, 2017.